Optics Communications 301–302 (2013) 67–73

Contents lists available at SciVerse ScienceDirect

Optics Communications

journal homepage: www.elsevier.com/locate/optcom

Spectral properties and synchronization scenarios of two mutually delay-coupled semiconductor lasers

D.A. Arroyo-Almanza [a,*], A.N. Pisarchik [a], I. Fischer [b], C.R. Mirasso [b], M.C. Soriano [b]

[a] Centro de Investigaciones en Optica, Loma del Bosque 115, Lomas del Campestre, 37150 Leon, Mexico
[b] Instituto de Física Interdisciplinar y Sistemas Complejos, IFISC (CSIC-UIB), Campus Universitat Illes Balears, E-07122 Palma de Mallorca, Spain

ARTICLE INFO

Article history:
Received 23 December 2012
Received in revised form
20 March 2013
Accepted 26 March 2013
Available online 16 April 2013

Keywords:
Semiconductor laser
Low frequency fluctuation
Synchronization
Optical injection
Nonlinear dynamics
Chaos

ABSTRACT

We experimentally study the intensity dynamics and the optical spectra of two similar mutually delay-coupled semiconductor lasers. While changing two relevant parameters of the coupled system, namely the bias currents and the coupling strength of the lasers, we observe significant modifications in the laser emission characterized via optical spectra, laser intensity dynamics, and cross-correlation functions. We find distinct synchronization scenarios for two bias currents: 1.02 and 1.25 times the threshold bias current of the solitary laser. Optical spectra in both cases strongly depend on the coupling strength between the lasers. For the low bias current and strong coupling, the lasers exhibit dynamical bistability, i.e. the coexistence of low-frequency fluctuations and stable continuous-wave emission.

1. Introduction

Semiconductor lasers (SLs) subject to delayed feedback, as well as motifs of delay-coupled SLs have attracted much attention due to their potential applications in different areas, such as high-power emission by diode laser arrays [1], quantum noise reduction [2], chaotic communications [3,4], random number generation [5–7], and information processing [8] (for a review see [9]). In delay-coupled SLs, even short coupling delay times (1 ns or smaller) cannot be neglected due to the laser's fast characteristic time scales [10–12]. If the time taken by the light to travel from one laser to the other is of the same order of or larger than the relaxation oscillation period, a very rich dynamical behavior including fully developed chaos, low-frequency fluctuations (LFF), and coexistence of LFF and stable emission can be observed. This scenario is similar to that detected in a laser with delay optical feedback [13,14].

Although many researchers considered unidirectionally coupled semiconductor lasers [3,15–18], there is also a strong interest in studying mutually coupled SLs [10–12,19–24] where some unexpected dynamical behaviors were found [21,22]. One prominent aspect is the occurrence of a spontaneous symmetry breaking [10,11,19] that gives rise to stable *generalized achronal synchronization* in two mutually delay-coupled SLs [10,19,24]. This generalized achronal synchronization state is particularly interesting because it originates from the bidirectional coupling of perfectly symmetric systems. *Identical isochronal (zero-lag) synchronization* only occurs when self-feedback is added to each laser [25,26] or another laser or a semitransparent mirror is placed between the two SLs [27,28]. Although many studies addressed the dynamical and synchronization properties of mutually delay-coupled SLs, only few works included the study of their optical spectral properties [29,30]. Interestingly, it was found that their spectra present features similar to those of a solitary SL with optical feedback [31–35]; in particular, a significant line broadening is detected when the lasers operate in a chaotic regime [33].

In this paper, we experimentally revisit the dynamical behavior of two very similar mutually delay-coupled SLs. Our study is motivated by the recent availability of a new generation of instruments, such as high-resolution optical analyzers and high-speed real-time digital oscilloscopes that enable the characterization of the dynamical properties of delay-coupled SLs with unprecedented precision. By analyzing the intensity dynamics and the highly resolved optical and frequency (rf) spectra, we study in detail the transition from stable continuous-wave (CW) regime to LFF, bistability (coexistence of LFF and CW) and chaos [14,36] when increasing the coupling strength. Particular attention is given to the synchronization of mutually coupled SLs in the regimes of LFF and coherence collapse. We also show that not only the laser dynamics but also the synchronization properties strongly depend on the laser bias currents.

* Corresponding author. Tel.: +52 477 4414200; fax: +52 477 4414209.
E-mail addresses: dianaa@cio.mx (D.A. Arroyo-Almanza), apisarch@cio.mx (A.N. Pisarchik), ingo@ifisc.uib-csic.es (I. Fischer), claudio@ifisc.uib-csic.es (C.R. Mirasso), miguel@ifisc.uib-csic.es (M.C. Soriano).

0030-4018/$ - see front matter © 2013 Elsevier B.V. All rights reserved.
http://dx.doi.org/10.1016/j.optcom.2013.03.040

2. Experimental setup

The experimental arrangement is shown in Fig. 1. We used two fiber-pigtailed discrete-mode semiconductor lasers (Eblana Photonics), both with a 1542 nm nominal emission wavelength. The lasers were selected from the same wafer in order to achieve well-matched parameters, and butterfly mounted with Thorlabs mount LM14S2. Both the pump current and the laser temperature were controlled and stabilized by a Thorlabs PRO800 module ITC8022 with an accuracy of ± 0.01 °C and ± 0.01 mA, respectively. The threshold current of the solitary laser 1 was $I_{th1}=11.28$ mA at 19 °C and that of laser 2 was $I_{th2}=11.85$ mA at 20 °C. As shown schematically in Fig. 1, the lasers were connected via 90/10 optical couplers (OC_1 and OC_2). About 90% of the output radiation was used for the coupling through a polarization controller (PC) to ensure parallel polarization and the remaining 10% was used for detection by fast photodiodes (D) (Miteq 12.5-GHz bandwidth). The signals from the photodiodes were analyzed with a frequency spectrum analyzer (Anritsu MS2667C with a 9 kHz to 30 GHz frequency range) and a fast oscilloscope (LeCroy WaveMaster 8 16Zi with a sampling rate of 40 Gsamples/s and 16-GHz analog bandwidth). The optical spectra were measured with a high-resolution optical spectrum analyzer (BOSA with a 10 MHz resolution). The coupling time was fixed to $\tau_c=nL/c=63$ ns; where $L=12.6$ m is the fiber length of the coupling path, c is the speed of light in vacuum, and $n=1.5$ the fiber refractive index. In order to protect the lasers from undesired feedback, an optical isolator (ISO) was located in front of each photodiode. The fiber connectors were of APC type (connector with angle polished) and had a return loss of about 50 dB.

The dynamics and synchronization properties of delay-coupled SLs depend on several parameters, including injected powers and detuning of the laser wavelengths. In order to control the amount of light coupled to the lasers, we placed an attenuator (A) by which we varied the transmission losses between the lasers. In our experiments, the maximum coupling was estimated by taking into account the coupling efficiency of the laser to the fiber that was approximately 75%, and to the optical couplers that was about 90% of transmission. Since we used two couplers and two fiber-pigtailed lasers, the whole coupling loss was about 45% ($0.75\times0.9\times0.9\times0.75$). For the overall coupling strength, we have to add an extra 10% loss in the fiber connectors and hence the estimated maximum coupling was about 40% of the emitted light. Maximum and minimum coupling correspond to attenuations of 0 dB and −34 dB of the laser emission, respectively.

Before exploring the dynamics of the two mutually coupled SLs, we ensured that the lasers were as similar as possible and operated under the same conditions. Both the bias current and the temperature of each solitary laser were adjusted such that the uncoupled lasers had the same emission wavelengths and the same relaxation oscillation frequencies. In the following sections, we study the laser dynamics for two different values of the bias currents: (i) when the laser is biased at $I=1.02\ I_{th}$, and (ii) when the laser is biased at $I=1.25\ I_{th}$, where I_{th} is the threshold current of the solitary lasers.

3. Laser behavior for $I=1.02\ I_{th}$

In this section we study the dynamics of the two mutually coupled SLs when the bias current is very close to the lasing threshold, specifically, at $I=1.02\ I_{th}$

3.1. Intensity dynamics, optical and rf spectra

Fig. 2 shows optical spectra, intensity time series, and frequency (rf) spectra for different attenuation values (k). Similarly to a SL with optical feedback [31], four distinct dynamical regimes are found depending on the coupling strength (or attenuation), that we describe as follows.

(i) The uncoupled and weakly coupled lasers operate in a noisy CW (stable steady state) regime characterized by a narrow spectral linewidth ($k=-34$ dB) [Fig. 2(a)]. (ii) As the attenuation is decreased ($k=-24$ dB), the lasers start to oscillate in a chaotic manner; this process is accompanied by the linewidth broadening [Fig. 2(b)]. Two dominant frequencies in the laser oscillations can be distinguished in the rf spectrum [right panel of Fig. 2(b)]. The frequency corresponding to the interference between compound cavity modes is about $1/2\tau_c$~7.9 MHz [see spacing between frequency peaks at the inset figure in the right panel of Fig. 2(b)], while the relaxation oscillation frequency of the coupled lasers is about 3 GHz. (iii) The linewidth further broadens when the injected power is increased, i.e., when the attenuation is decreased ($k=-10$ dB). The maxima in the optical and rf spectra shift toward smaller frequencies [Fig. 2(c)]. This regime, known as coherence collapse, is characterized by a significant linewidth broadening by several orders of magnitude (to about 20 GHz) [33,37]. The laser oscillations again show two dominant frequencies. (iv) At very strong coupling ($k=-2$ dB), bistability emerges [14,36]. The lasers operate either in the regime of LFFs [Fig. 2(d)] or in a stable steady state of the compound cavity (CW regime) [Fig. 2 (e)]. These two stable states alternate in time due to the influence of spontaneous emission and carrier noise. In the steady state regime, the coherence of the lasers is regained, but the optical frequency is shifted toward smaller frequencies compared to the solitary lasers and the relaxation oscillations are strongly suppressed.

3.2. Synchronization

The synchronization of two lasers can be characterized by the cross-correlation function [38]:

$$C(\Delta t)=\frac{\langle[P_1(t)-\langle P_1\rangle][P_2(t+\Delta t)-\langle P_2\rangle]\rangle}{\{\langle[P_1(t)-\langle P_1\rangle]^2\rangle\langle[P_2(t)-\langle P_2\rangle]^2\rangle\}^{1/2}} \quad (1)$$

where P_1 and P_2 are the output powers of laser 1 and laser 2, respectively. Angle brackets $\langle\ \rangle$ denote time average, and Δt is the time shift. Fig. 3 shows the time series (left), synchronization diagram (middle), and cross-correlation (right) between strongly coupled SLs ($k=-4$ dB) operating in the LFF regime. The synchronization diagram is constructed by plotting the intensity of laser 1 versus the intensity of laser 2 after compensating for the

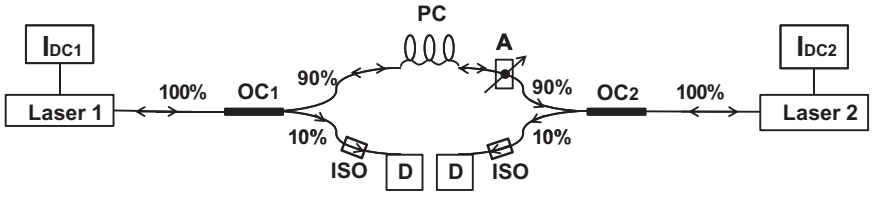

Fig. 1. Experimental setup of two mutually coupled semiconductor lasers. I_{DC1} and I_{DC2} are laser current and temperature controllers, OC_1 and OC_2 are optical couplers, PC is a polarization controller, A is a variable attenuator, ISO are optical isolators, and D are photodetectors. All components are connected via optical fibers.

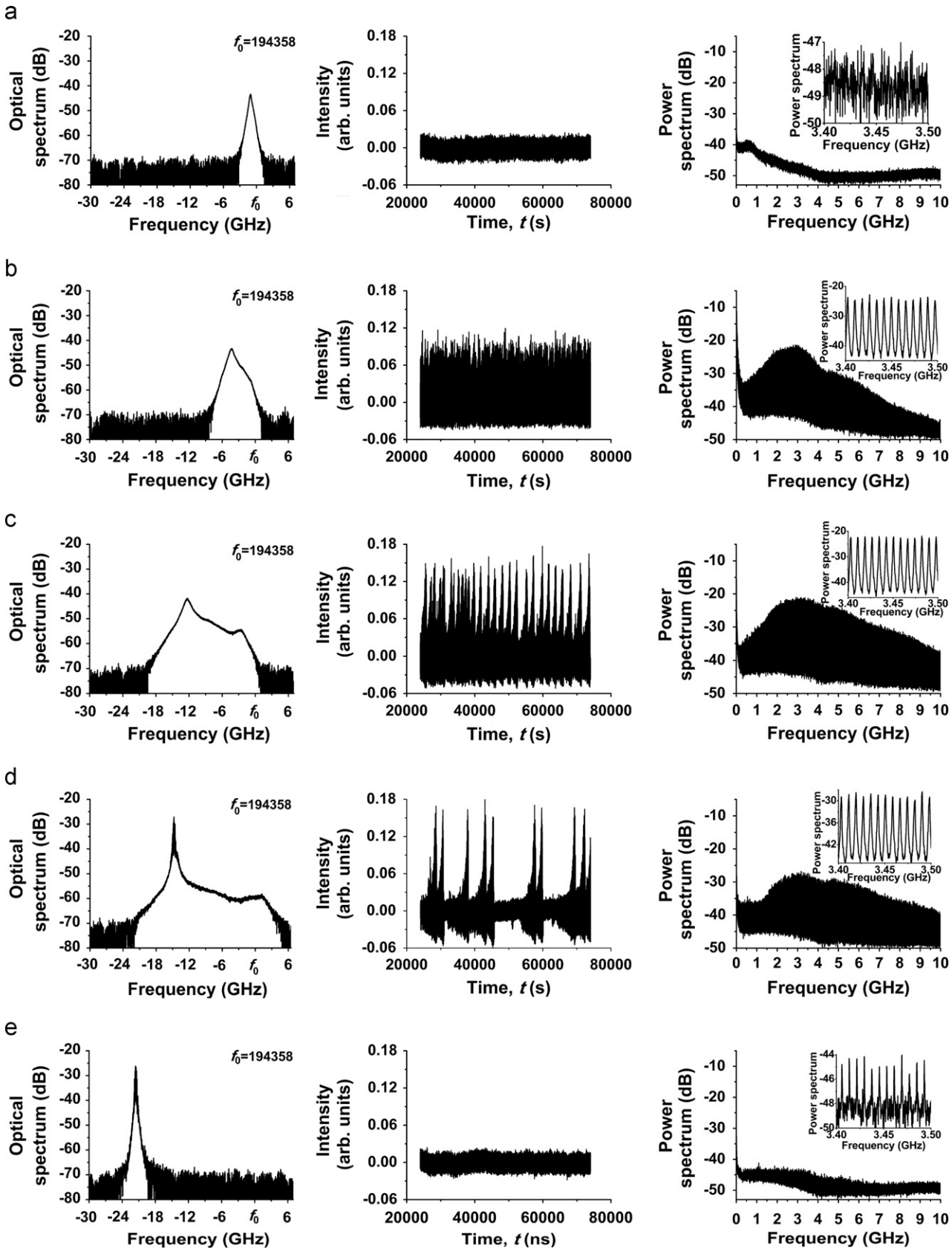

Fig. 2. Optical spectra (left), time series (middle), and rf spectra (right) for different attenuation values: (a) –34 dB, (b) –24 dB, (c) –10 dB, (d) –2 dB, and (e) –2 dB (CW). The insets in the rf spectra show an enlargement around 3.45 GHz in order to visualize the frequency peaks corresponding to the interference between compound cavity modes.

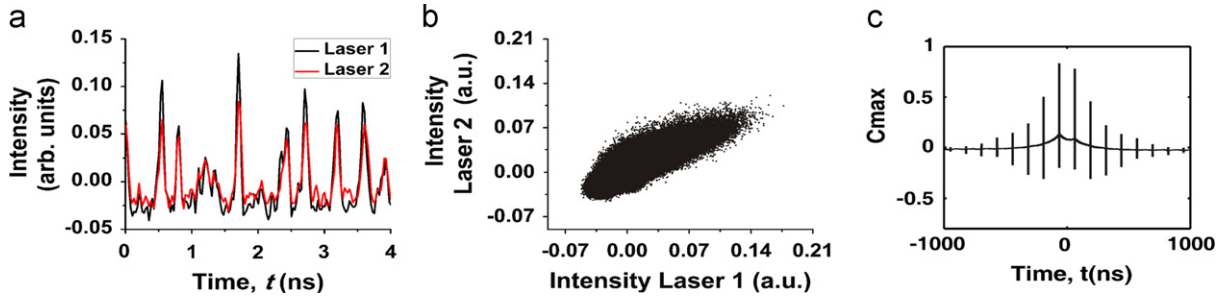

Fig. 3. Time series (left), synchronization diagram (middle), and cross-correlations (right) between two lasers for $k=-4$ dB demonstrating achronal synchronization. The time lag is compensated in both the time series and synchronization diagram.

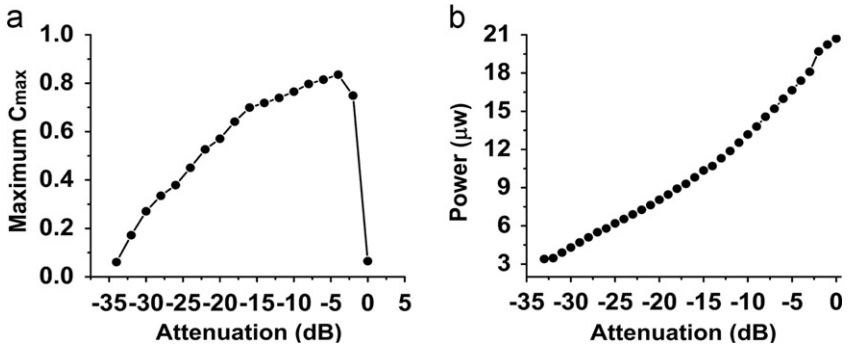

Fig. 4. (a) Maximum cross-correlation C_{max} between lasers and (b) average power of one of the lasers as functions of attenuation.

coupling time. It provides an indication of the synchronization quality, even though we refer to generalized synchronization here; a high degree of synchronization results in a diagram that orders around a 45-degree line. The two maxima in the cross-correlation function (right panel) occur at time lags equal to $\pm\tau_c=63$ ns. For $k=-4$ dB, the maximum cross-correlation coefficient is $C_{max}=0.83$, indicating stable achronal synchronization.

Fig. 4 depicts the maximum of the cross-correlation coefficient and the average emitted power as functions of the attenuation. As the attenuation is decreased, C_{max} increases up to its maximum value of 0.83. Then, in the large coupling region, C_{max} drops to almost zero when the lasers switch to a noisy stable steady state of the compound cavity. The average emitted power increases with an increasing attenuation, even when the lasers are in the bistable regime.

4. Laser behavior for $I=1.25\ I_{th}$

In this section, we study the laser dynamics and synchronization properties of the mutually coupled SLs when the bias current is set at $I=1.25\ I_{th}$.

4.1. Intensity dynamics, optical and rf spectra

The laser' temporal and spectral dynamics are different from that observed in the previous case of lower current ($I=1.02\ I_{th}$). Fig. 5 shows the optical spectra of the uncoupled lasers, which are almost identical. They exhibit the characteristics of single mode emission with relaxation oscillation sidebands.

The optical spectra for different attenuations are shown in Fig. 6. For the maximum value of attenuation (−36 dB) we can see in Fig. 6(a) that the lasers exhibit the characteristics of single mode emission with relaxation oscillation sidebands as the optical spectra of the uncoupled laser. When the attenuation is decreased, we observe undamped relaxation oscillations [Fig. 6(b,c)] and a

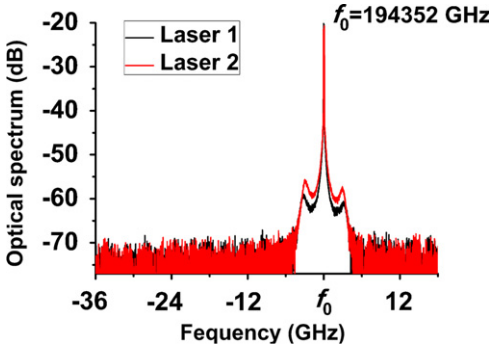

Fig. 5. Optical spectra of solitary lasers.

transition to chaotic emission with multiple compound cavity modes, resulting in the significant linewidth broadening [Fig. 6 (d,e)]. Similarly to the case of the low bias current, the spectrum shifts toward smaller frequencies (longer wavelengths) [Fig. 6(f,g)]. Interestingly, the optical spectrum for 0-dB attenuation [Fig. 6(h)] shows two distinct spectral contributions, around the solitary laser frequency and the modes with higher optical gain, respectively.

Fig. 7 shows typical rf spectra for different attenuation values. The dominant frequencies are 2.77 GHz, 2.66 GHz, 2.81 GHz, and 2.3 GHz for −36 dB, −30 dB, −24 dB, and 0 dB, respectively. It can be seen that even for high attenuation, the lasers exhibit undamped relaxation oscillations [see Fig. 7(a)]. For an attenuation of −30 dB we can see clearly that the frequencies spaced by ~7.9 MHz correspond to the interference between compound cavity modes, the contribution of these frequency peaks is significant and these peaks are distributed in a rather regular way [see the inset in Fig. 7(b)]. For smaller attenuation ($k=-24$ dB) the power is more distributed along the different frequency components and the compound cavity peaks structure is more irregular [see the inset in Fig. 7(c)]. The distribution of power over a wider frequency range is accompanied by the significant spectral broadening [Fig. 7(c)] that suggests an increasing complexity (chaoticity)

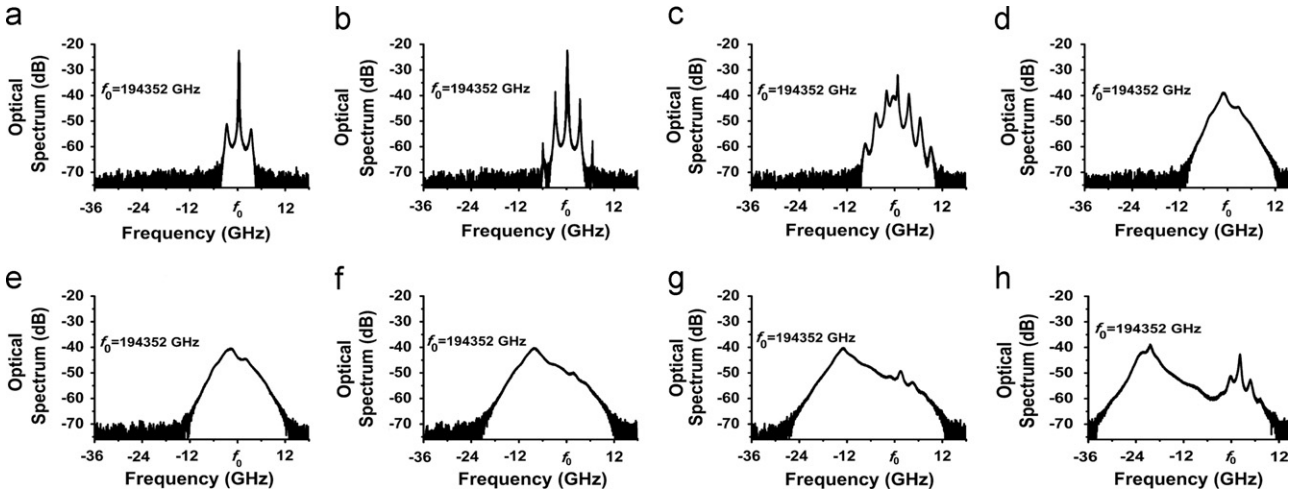

Fig. 6. Optical spectra for different attenuation values: (a) −36 dB; (b) −34 dB; (c) −30 dB; (d) −24 dB; (e) −20 dB; (f) −10 dB; (g) −6 dB and (h) 0 dB.

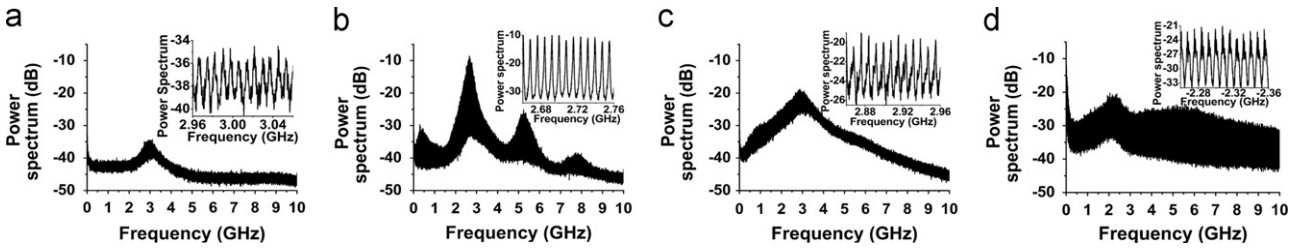

Fig. 7. rf spectra for different attenuation: (a) −36 dB; (b) −30 dB; (c) −24 dB and (d) 0 dB. The insets show enlarged parts of the rf spectra close to the maxima.

of the laser oscillations. For very low attenuation, the contribution of the compound cavity modes is very strong, thus further increasing the system complexity [Fig. 7(d)].

4.2. Synchronization

Fig. 8 shows the laser time series (left panels), the corresponding synchronization diagrams (middle panels), and the cross-correlation functions (right panels) *for* $I=1.25\ I_{th}$. The lasers display different synchronization states for different attenuation values. For the maximum value of attenuation (−36 dB) the maximum cross-correlation is $C_{max}=0.12$, indicating that the lasers oscillate very asynchronously [Fig. 8(a)].

For high attenuation (between −36 dB and −30 dB), *intermittent achronal synchronization* is observed [Fig. 8(b)]. In this regime the lasers are synchronized only in the windows of large-amplitude oscillations, whereas in the zones of low-amplitude oscillations the lasers oscillate asynchronously. The complex fine structure in the figure of the cross-correlation reflects this synchronization state. For an attenuation of −30 dB, the lasers become continuously synchronized and the cross-correlation reaches its maximum value ($C_{max}=0.82$) [Fig. 8(c)]. For this attenuation, *achronal synchronization* is observed with a pronounced maximum in the cross-correlation function.

For stronger coupling ($k=-20$ dB) [Fig. 8(d)], the maximum of the cross-correlation decreases until $C_{max}=0.21$, indicating that the synchronization is being lost. Finally, for the minimum attenuation value of 0 dB (maximum coupling), we observe stable achronal synchronization [Fig. 8(e)]. Unlike the case of the bias current close to the threshold, for this higher current we do not observe bistability.

In Fig. 9, we plot the maximum cross-correlation and the average output power versus the attenuation. Interestingly, the maximum cross-correlation depends non-monotonously on the attenuation and four qualitatively different regions can be distinguished. As observed in the case of very low bias current, for the strongest attenuation the lasers oscillate asynchronously (see point *a* in Fig. 9).

In the region ($\overline{ab}$), intermittent achronal synchronization is observed. As the attenuation is decreased, the average cross-correlation increases because the windows of synchronization become longer. For an attenuation of −30 dB (at point *b*), the lasers are all the time well synchronized. In the region ($\overline{bc}$), the cross-correlation decreases, i.e. synchronization degrades. This decrease in the cross-correlation is associated with the transition from weak to strong chaos recently reported in [39,40]. In the region ($\overline{cd}$), the maximum of the cross-correlation increases with decreasing attenuation, i.e., the almost uncorrelated state observed at point *c* gives rise to a highly-synchronized state (illustrated at point *d*). This increase in the cross-correlation is associated with the transition from strong back to weak chaos [39,40]. The high degree of synchronization remains up to the minimum attenuation, depicted as point *e*. The cross-correlation saturates around 0.75 and does not change in the region ($\overline{de}$). It is important to note that complete synchronization is never achieved. It can be seen in Fig. 9(b) that the average power increases monotonously with decreasing attenuation as in the case for low bias current.

5. Discussion and conclusion

We have experimentally investigated the spectral and temporal characteristics of two mutually delay-coupled semiconductor lasers. By exploring the coupling strength dependence for two different values of the bias current: 1.02 and 1.25 times the threshold bias current of the solitary laser, we have found different dynamical regimes and different synchronization states. For the

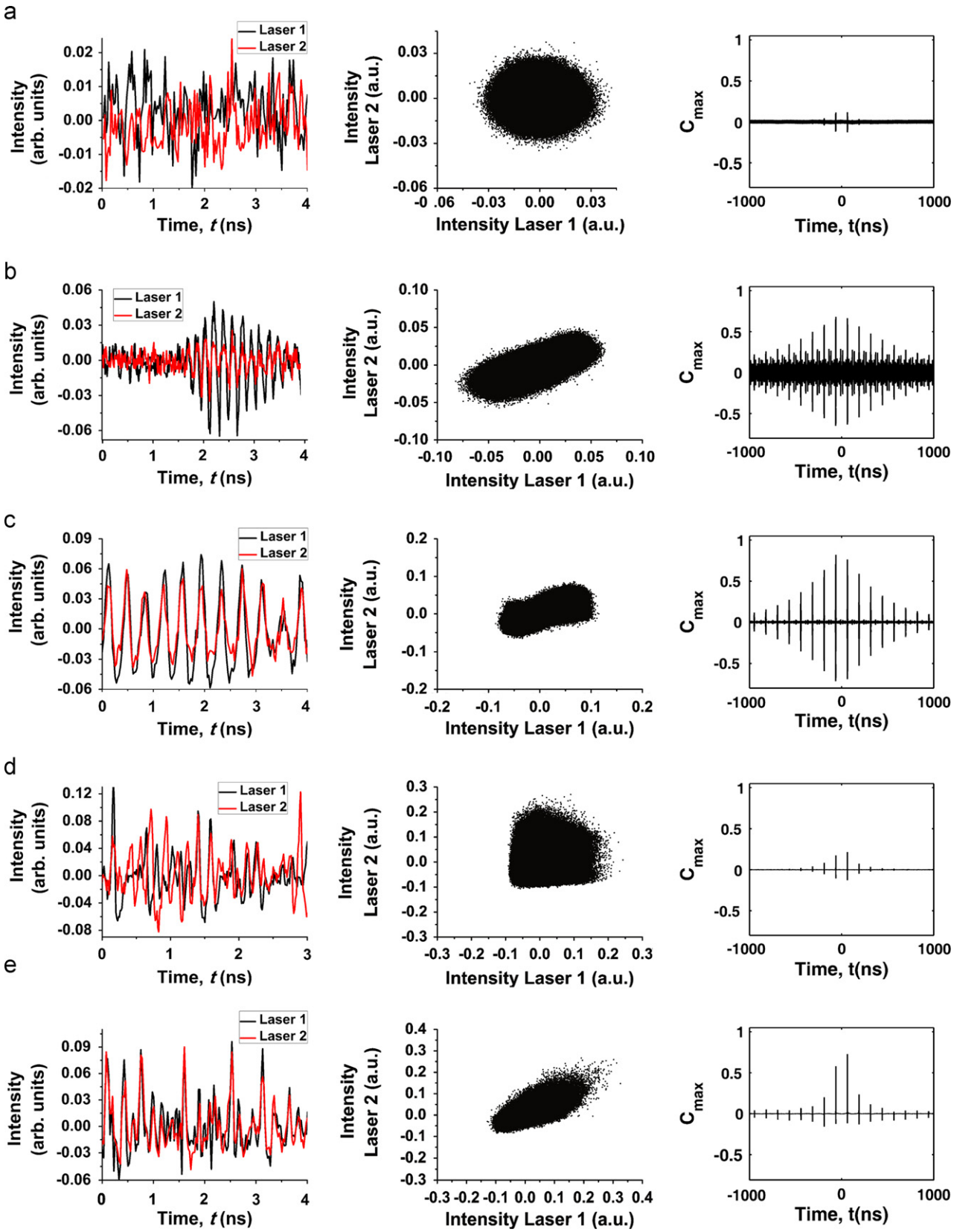

Fig. 8. Time series of laser intensities (left) and synchronization diagrams with compensated coupling time (middle), and cross-correlation (right) for different attenuations: (a) −36 dB, and (b) −34 dB, (c) −30 dB and, (d) −20 dB, and (e) 0 dB.

low injection current ($I=1.02\ I_{th}$), we observed that the maxima of the cross-correlation function increased with decreasing attenuation between the lasers. For low attenuation (strong coupling), we found the coexistence of LFF and CW regimes; these two regimes alternated in time due to spontaneous emission and carrier noise. Although the coupled lasers exhibited stable emission, their

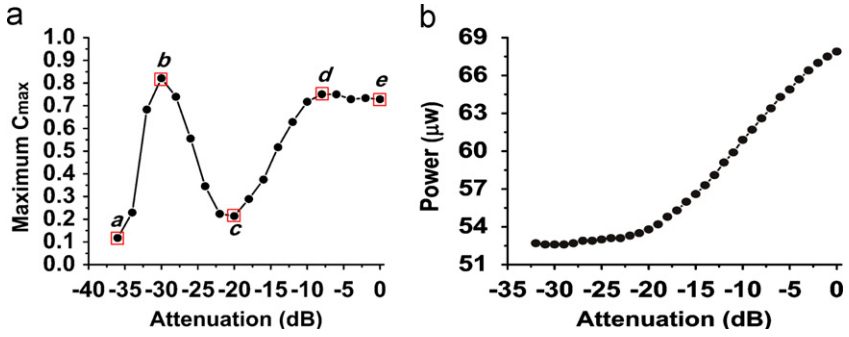

Fig. 9. (a) Maximum cross-correlation between lasers and (b) average power of one of the lasers versus attenuation.

optical spectra were different from those of the solitary lasers; the central frequency of the coupled lasers was shifted toward lower frequencies, corresponding to the stable high gain compound cavity modes. The average power of the lasers increased as the attenuation was decreased, independently of the changes in the dynamical regime.

The dynamics was more complex when the lasers were operated at higher bias currents ($I=1.25\ I_{th}$). A transition to chaotic emission with multiple compound cavity modes and a significant linewidth broadening were observed when the attenuation was decreased. Different synchronization states were identified for different attenuation values. Interestingly, the maximum cross-correlation between the lasers' intensities changed non-monotonously as the attenuation factor was decreased. For low couplings the cross-correlation increased from 0.12 to 0.82; it decreased to 0.21 for intermediate coupling values and then again increased until it saturates to about 0.75 for large couplings. The qualitative changes in this dependence were associated with changes in the dynamical regimes. Correlation degraded in the strong chaos dynamical regime, while the maximum correlation was larger in the weak chaos regions. However, we did not find significant differences in the maximum values of cross-correlation for strongly coupled lasers, when the laser was pumped at the 1.02- and 1.25-threshold currents. In both cases stable achronal synchronization was observed. Regarding synchronization, the weakly coupled lasers were intermittently synchronized in time. The lasers were synchronized only in those temporal windows with large-amplitude spikes, while they oscillated asynchronously in windows with low-amplitude spikes. For smaller attenuations, the lasers were continuously synchronized but, due to the increasing complexity of the coupled system, they lost synchronization. For strong coupling (very low attenuation, 0 dB to −12 dB) they synchronized again in the generalized achronal synchronization state. Unlike the case of low bias current, for higher bias current we did not observe bistability between chaotic pulsations and CW emission.

Acknowledgments

D.A. Arroyo-Almanza and A.N. Pisarchik express their gratitude to the Consejo Nacional de Ciencia y Tecnologia (CONACYT) for the financial support through project no. 100429. Also, this work was partially supported by MICINN (Spain), Comunitat Autònoma de les Illes Balears, MINECO and FEDER, under projects FIS2007-60327 (FISICOS), TEC2009-14101 (DeCoDicA), Grups Competitius, FIS2012-30634 (INTENSE@COSYP) and TEC2012-36335 (TRIPHOP).

References

[1] J.R. Leger, M.L. Scott, W.B. Veldkamp, Applied Physics Letters 52 (1988) 1771.
[2] E.C. Serrat, M.C. Torrent, J. García-Ojalvo, R. Villaseca, Physical Review A 64 (2001) 041802.
[3] S. Donati, C.R. Mirasso, IEEE Journal of Quantum Electronics 38 (2002) 1138.
[4] A. Argyris, D. Syvridis, L. Larger, V. Annovazzi-Lodi, P. Colet, I. Fischer, J. García-Ojalvo, C.R. Mirasso, L. Pesquera, K.A. Shore, Nature 438 (2005) 343.
[5] A. Uchida, K. Amano, M. Inoue, K. Hirano, S. Naito, H. Someya, I. Oowada, T. Kurashige, M. Shiki, S. Yoshimori, K. Yoshimura, P. Davis, Nature Photonics 2 (2008) 728.
[6] I. Reidler, Y. Aviad, M. Rosenbluh, I. Kanter, Physical Review Letters 103 (2009) 24102.
[7] N. Oliver, M.C. Soriano, D.W. Sukow, I. Fischer, Optics Letters 36 (2011) 4632.
[8] D. Brunner, M.C. Soriano, C.R. Mirasso, I. Fischer, Parallel photonic information processing at gigabyte per second data rates using transient states, Nature Communications 4 (2013) 1364.
[9] M.C. Soriano, J. Garcia-Ojalvo, C.R. Mirasso, I. Fischer, Reviews of Modern Physics 85 (2013) 421.
[10] T. Heil, I. Fischer, W. Elsäer, J. Mulet, C.R. Mirasso, Physical Review Letters 86 (2001) 795.
[11] H. Fujino, J. Ohtsubo, Optical Review 8 (2001) 351.
[12] T. Heil, I. Fischer, W. Elsäer, Physical Review A. 58 (1998) R2672.
[13] G.H.M. van Tartwijk, D. Lenstra, Quantum and Semiclassical Optics 7 (1995) 87.
[14] T. Heil, I. Fischer, W. Elsäer, Physical Review A 60 (1999) 634.
[15] V. Ahlers, U. Parlitz, W. Lauterborn, Physical Review E 58 (1998) 7208.
[16] C. Masoller, Physical Review Letters 86 (2001) 2782.
[17] I. Wedekind, U. Parlitz, International Journal of Bifurcation and Chaos 11 (2001) 1141.
[18] J.M. Buldú, R. Vicente, T. Pérez, C.R. Mirasso, M.C. Torrent, J. García-Ojalvo, Applied Physics Letters 81 (2002) 5105.
[19] J. Mulet, C. Mirasso, T. Heil, I. Fischer, Journal of Optics B: Quantum and Semiclassical Optics 6 (2004) 97.
[20] H. Erzgräber, D. Lenstra, B. Krauskopf, Optics Communications 255 (2005) 286.
[21] A. Hohl, A. Gavrielides, T. Erneux, V. Kovanis, Physical Review Letters 78 (1997) 4745.
[22] A. Hohl, A. Gavrielides, T. Erneux, V. Kovanis, Physical Review A 59 (1999) 3941.
[23] N. Gross, W. Kinzel, I. Kanter, M. Rosenbluh, L. Khaykovich, Optics Communications 267 (2006) 464.
[24] J.K. White, M. Matus, J.V. Moloney, Physical Review E 65 (2002) 036229.
[25] E. Klein, N. Gross, M. Rosenbluh, W. Kinzel, L. Khaykovich, I. Kanter, Physical Review E 73 (2006) 066214.
[26] E.A. Viktorov, A.M. Yacomotti, P. Mandel, Journal of Optics B: Quantum and Semiclassical Optics 6 (2004) L9.
[27] I. Fischer, V. Raul, J. Buldú, M. Peil, C. Mirasso, M. Torrent, J. García-Ojalvo, Physical Review Letters 97 (2006) 123902.
[28] R. Vicente, C.R. Mirasso, I. Fischer, Optics Letters 32 (2007) 403.
[29] F. Rogister, M. Blondel, Optics Communications 239 (2004) 173.
[30] T. Deng, G. Xia, Z. Wu, X. Lin, J. Wu, Optics Express 19 (2011) 8762.
[31] R.W. Tkach, A.R. Chraplyvy, Journal of Lightwave Technology LT-4 (1986) 1655.
[32] L. Goldberg, H.F. Taylor, A. Dandridge, J.F. Weller, R.O. Miles, IEEE Journal of Quantum Electronics QE-18 (1982) 555.
[33] G.A. Acket, D. Lenstra, A.J. Den Boef, B.H. Verbeek, IEEE Journal of Quantum Electronics QE-20 (1984) 1163.
[34] J. Mørk, B. Tromborg, J. Mark, IEEE Journal of Quantum Electronics 28 (1992) 93.
[35] G. Van der Sande, M.C. Soriano, I. Fischer, C.R. Mirasso, Physical Review E 77 (2008) 055202.
[36] J. Mørk, B. Tromborg, P.L. Christiansen, IEEE Journal of Quantum Electronics QE-24 (1988) 123.
[37] J. Wang, K. Petermann, IEEE Journal of Quantum Electronics QE-27 (1991) 3.
[38] M.C. Soriano, F. Ruiz-Oliveras, P. Colet, C.R. Mirasso, Physical Review E 78 (2008) 046218.
[39] S. Heiligenthal, T. Dahms, S. Yanchuk, T. Jüngling, V. Flunkert, I. Kanter, E. Schöll, W. Kinzel, Physical Review Letters 107 (2011) 234102.
[40] S. Heiligenthal, T. Jüngling, O. D'Huys, D.A. Arroyo-Almanza, M.C. Soriano, I. Fischer, I. Kanter, W. Kinzel, arXiv:1210.1887.